This is the accepted version of the manuscript.

SARS CoV-2 Aerosol: How far it can travel to the lower airways?

Mohammad S. Islam[1]*, Puchanee Larpruenrudee[1], Akshoy R. Paul[2], Gunther Paul[3], Tevfik Gemci[4], Yuantong Gu[5] and Suvash C. Saha[1*]

[1]School of Mechanical and Mechatronic Engineering, University of Technology Sydney (UTS), 15 Broadway, Ultimo, NSW-2007, Australia

[2]Department of Applied Mechanics, Motilal Nehru National Institute of Technology Allahabad, Prayagraj 211004, Uttar Pradesh, India

[3]James Cook University, Australian Institute of Tropical Health and Medicine, Townsville, QLD 4810, Australia

[4] Synergy CFD Consulting, Las Vegas, NV 89146, USA

[5]School of Mechanical, Medical and Process Engineering, Faculty of Engineering, Queensland University of Technology, Brisbane-4000, Australia.

Corresponding Author: mohammadsaidul.islam@uts.edu.au; Suvash.Saha@uts.edu.au

Abstract

The recent outbreak of the SARS CoV-2 virus causes a significant effect on human respiratory health around the world. The contagious disease infected a large proportion of the world population resulting in long-term health issues and an excessive mortality rate. The SARS CoV-2 virus can spread as small aerosols and enters into the respiratory systems through the

oral (nose or mouth) airway. The SARS CoV-2 particle transport to the mouth-throat and upper airways is analysed by the available literature. Due to the tiny size, the virus can travel to the terminal airways of the respiratory system and form a severe health hazard. There is a gap in the understanding of the SARS CoV-2 particle transport to the terminal airways. The present study investigated the SARS CoV-2 virus particle transport and deposition to the terminal airways in a complex 17-generation lung model. This first-ever study demonstrates how far SARS CoV-2 particle can travel in the respiratory system. ANSYS Fluent solver was used to simulate the virus particle transport during sleep, light and heavy activity conditions. Numerical results demonstrate that a higher percentage of the virus particles are trapped at the upper airways when sleeping and in a light activity condition. More virus particles have lung contact in the right lung than the left lung. A comprehensive lobe specific deposition and deposition concentration study was performed. The results of this study provide a precise knowledge of the SARs CoV-2 particle transport to the lower branches and could help the lung health risk assessment system.

Keywords: SARS CoV-2, Terminal airways, Virus transport, 17-Generation lung.

Introduction

thoracic cavity and consists of inhalation and exhalation processes. During inhalation, airborne pollutants, as for example, particulate matter, dust, smoke, pollens, viruses, or allergens, often in the form of liquid droplets and aerosols are ingested into the airways. Aerosol is a term first introduced in the 1920s and was initially used in the context of therapeutic inhalation (Anderson, 2005).

The inhaled air is ingested into the respiratory tract, commonly termed as human airways, which has a complicated geometry and hence is difficult to reconstruct even using computerised modelling. Due to lack of CT-scan images, earlier researchers (Weibel, 1963;

Philips and Kaye, 1995; Kitaoka et al., 1999) used simplified (often with a regular cross-sectional shape) geometry of human airways. With the sophisticated imaging techniques, the researchers started developing more realistic geometry of human airways incorporating lung intricate shapes and minuscule anatomical features (Martonen et al., 1995; Lizal et al., 2012; Srivastav et al., 2013; Frederix et al., 2018) for conducting various computational studies. These studies include the effects of breathing through nasal and oral passages (Fitzpatrick et al., 2003), transmission and deposition of inhaled aerosols, fine and ultrafine particles etc. within the both upper and tracheobronchial airways (Fernández Tena and Casan Clarà, 2012; Mortazavi et al., 2020). In the last two decades, respiratory fluid dynamics has matured enough to allow multiscale, multiphysics modelling (Burrowes et al., 2008; Pozin, 2017) to analyse the various aspects of respiratory mechanics, starting from the inhalation mechanism (Islam et al., 2020) to aerosol (Xi and Longest, 2007; Islam et al., 2017; Lizal et al., 2020) and drug delivery through pulmonary routes (Heyder, 2004; Kleinstreuer et al., 2008) and even diseased airways (Martonen et al., 2003; Srivastav et al., 2014).

Refer to the term of aerosol, it is the combination between solid or liquid particles which are suspended in gas. Airborne transmission of many viral diseases is caused due to propagation of such airborne particles containing saliva, mucus, salts, cells and even infectious pathogens-viral and/or bacterial particles (Wells, 1955). The droplets are often originated from the viral infected inner epithelial layers of the respiratory tract surfaces (Mason, 2020) through exhalation, coughing, sneezing, talking, or vomiting by an infected person (Atkinson et al., 2009). The ongoing COVID-19 pandemic has triggered the publication of numerous research articles encompassing various aspects and behaviour of the SARS CoV-2 virus (Zhou and Zou, 2021). The virus mainly attacks human lung airways and eventually damages lung capacity of gas exchange (Mason, 2020). Hence, the study of the transport of SARS CoV-2 aerosol to the tracheobronchial airways (termed as lower airways) is important.

Prather et al. (2020) suggested that pulmonary infections are caused by small aerosols. Virus particle can suspend in air for longer period and can be transmitted from an infected person to a non-infected person. Larger virus particle, on the other hand, can survive on the surfaces for longer period and can be transmitted through contacts (Bhardwaj and Agrawal, 2020a, 2020b). Kumar and Lee (2020) adopted continuous phase modelling for smaller aerosols, while discrete phase simulation was conducted for the larger aerosols. Diffusion equation-based Monte-Carlo modelling was used by Vuorinen et al. (2020) for the transport of virus aerosols. Appropriate source and sink terms are added to the diffusion transport equations to represent the variable location of the infected people and source of ventilation, respectively. Xie et al. (2009) stressed the importance of including droplet distribution (i.e. variation in size) for discrete phase modelling since it is connected to the travelling path as well as the chances of viral infections (called viral load) in case of SARS CoV-2. Liquid particles evaporation is another important phenomenon while transmitting the virus-laden aerosols, which is dependent on ambient temperature and saturation pressure. A recent study reported in the literature that small droplets released from the exhalation may be laden with Covid-19 virus has very short evaporation time scale ($\leq$ 1s) and hence are evaporated as soon as it is ejected. Hence, the virus is considered as a particle (Chaudhuri et al. 2020). The larger droplet or virus-laden particles are larger and cannot travel to the lower airways, as larger particles usually deposit to the upper airways. A recent study (Kwee and Kwee 2020a) showed that nano-sized SARS CoV-2 Aerosol are deposited to various lobes of the lung in their radiographic images, which supports the assumption of this study. However, after inhalation the evaporation is largely regulated by the body temperature. Recently, a number of researchers (Feng et al., 2020; Chaudhuri et al., 2020, de Oliviera et al., 2021) investigated various aspects of liquid particles evaporation and transmission in light of the COVID-19 pandemic. Smaller aerosols generated from continuous speech in a poorly ventilated room increased the infection risk by 11% as revealed in a recent

97 study (de Oliviera et al. 2021) and hence reiterates the importance of maintaining proper
98 ventilation and physical distancing to avoid infection transmission.

99 With the outbreak of Covid-19 pandemic, a few researchers have also worked on the virus
100 transmission in human airways. Balázs et al. (2020) employed a lung model based on a
101 stochastic deposition, which was developed by Koblinger and Hofmann (1990) to find out the
102 deposition of viral loads and revealed that over 60% of the inhaled viral masses were
103 deposited in the extrathoracalis (upper) which are the portion of the human lung airways, and

104 suggested to affect the upper airways and if not diagnosed, could eventually develop into
105 pneumonia. Other researchers focused on aerosol behaviour in the intra-distal region of a
106 simplistic lung model in the presence of different breathing conditions (Ciloglu, 2020), gravity
107 and surface tension effects on micro-bubbles in simplistic bifurcated airways (Munir and Xu,
108 2020), mask-wearing effects in upper respiratory geometry (Xi et al., 2020), aerosol transport
109 in phantom lung bronchioles (Mallik et al., 2020), cough exhalation from a 18-generation
110 simplistic airways (Si et al., 2021) etc.

111 The review of literature reveals a plethora of works on the transmission of infections
112 and exhalation behaviour originated from oral and nasal openings of the human airways.
113 However, the transportation of virus- aerosols to the tracheobronchial human airways involving
114 a realistic and detailed geometry of the airways has not yet discussed and analysed in detail.
115 Since empirical evidence of SARS CoV-2 attacking the respiratory organ in the COVID-19
116 infected population exists, a CFD investigation of virus aerosol transport in a realistic human
117 airways up to the 17th generation would help medical practitioners and inform further
118 diagnosis and prognosis of the COVID-19 disease. The CFD studies of airflow and CoV-2
119 virus deposition in a digital reference model of the 17-generation airway were based on the
120 anatomical model of an adult male, free of pathological alterations by Schmidt et al. (2004).
121 The lung model consists 1453 bronchi up to the 17^{th} Horsfield order.

Numerical Methods

The numerical study solved the air and particle transport equations and analysed the particle flow in first 17-bifurcatins of the human lung. The Lagrangian scheme and Finite Volume based discretisation techniques are used for this study. The numerical calculation method in this study is performed and conducted based on ANSYS 19.2 (FLUENT). The governing equations are solved as following;

$$\nabla.(\rho\vec{v}) = 0 \tag{1}$$

$$\nabla.(\rho\vec{v}\vec{v}) = -\nabla p + \nabla.(\mu(\nabla\vec{v} + \nabla\vec{v}^{T})) + \rho\vec{g} \tag{2}$$

where, static pressure is p, gravitational body force $\rho\vec{g}$, molecular viscosity μ.

The internal energy equation is

$$\nabla \cdot (\rho\vec{v}\mathrm{e}) = -\nabla \cdot \vec{J} \tag{3}$$

where e is the specific internal energy. The heat flux vector $\vec{J}$ is the sum of contributions due to heat conduction and enthalpy diffusion effects.

The inlet condition and velocity profiles are highly complex and irregular for person to person. No proper velocity profiles are established by the available literature. However, the flow inside the airway is similar to internal pipe flow and the flow become parabolic at the tracheal area of the airway. This study only considers the simulation which starts from trachea to lower generations of the human lung as well as the trachea wall which is considered as the inlet of the airway. Therefore, a fully developed parabolic inlet condition (White 2003) is used

$$u(r) = 2u_{av}(1 - \frac{r^2}{R^2}) \tag{4}$$

where R is the pipe radius. The corresponding velocity for 7.5 lpm, 15 lpm and 30 lpm cases are 0.4916 m/s, 0.9829 m/s and 1.996 m/s, respectively, which is the maximum velocity. For fully developed condition, maximum velocity is double of the average velocity.

SARS CoV-2 particle are smaller in size and it's approximately around 120 nm.

147 **(https://www.pptaglobal.org/media-and-information/ppta-statements/1055-2019-novel-**
148 **coronavirus-2019-ncov-and-plasma-protein-therapies).**

149 Therefore, nano-particle transport equations are solved (Inthavong, Tu and Ahmadi 2009).

$$\frac{du_i^p}{dt} = F_D + F_{Brownian} + F_{Lift} + \frac{\rho_p - \rho_g}{\rho_p} g_i$$

150 $$F_D = \frac{1}{C_c} C_D A_p \frac{\rho_g \left| u_i^g - u_i^p \right| (u_i^g - u_i^p)}{2m_p} = \frac{18\mu_g}{\rho_p d_p^2 C_c} (u_i^g - u_i^p) \quad (5)$$

$$C_c = 1 + \frac{2\lambda}{d_p}(1.257 + 0.4e^{\frac{-0.11 d_p}{2\lambda}})$$

151 where F_D is the drag force per unit particle mass m_p, C_D is the drag coefficient, A_p is the cross
152 sectional area of the particle, and C_c is the Cunningham correction factor. λ is the mean free path of
153 the gas molecules. u_i^p is the i-th component of the time-averaged particle velocity while u_i^g is the i-th
154 component of the time-averaged gas (air) velocity. ρ_p and ρ_g are the density of particle material and
155 gas (air), respectively. g_i is the gravitational component. μ_g denotes the gas (air) viscosity and d_p is
156 defined as particle diameter. For the low particle Reynolds number ($\mathrm{Re}_p < 0.5$), the drag coefficient
157 C_D can be defined as (Haider and Levenspiel 1989);

158 $$C_D = \frac{24}{Re_p}, \qquad Re_p < 0.5 \quad (6)$$

159 The particle Reynolds number can be calculated from,

160 $$Re_p = \rho_g \frac{d_p |u_r|}{\mu_g} \quad (7)$$

161 where, u_r is the relative velocity. The particle Re for 120nm particle for this study is 0.0168.
162 Amplitude for Brownian force is applied as

163 $$F_{Brownian} = \zeta \sqrt{\frac{\pi S_0}{\Delta t}} \quad (8)$$

164 where ζ is the unit variance for independent Gaussian random number, time-step integration of
165 the particle Δt. The spectral intensity (S_0) is defined as

$$S_o = \frac{216\mu k_B T}{\pi^2 \rho_p d_p{}^5 (\frac{\rho_p}{\rho_g})^2 C_c} \quad (9)$$

T is the fluid in absolute temperature, k_B is the Boltzmann constant, ρ_g is the gas density.

SIMPLE coupling scheme, and second order pressure discretisation technique are employed. Second order upwind technique is utilised for energy and momentum equations. Hybrid initialisation and pressure-based solver are used. The present model has considered the particle with a density of 1.0 g/cm^3; all particles were initiated from the one inlet area that was the trachea. Steady injection method is used. In reality, SARS-CoV-2 particles are spherical in shape like other viruses (https://www.nih.gov/news-events/nih-research-matters/novel-coronavirus-structure-reveals-targets-vaccines-treatments). Goldsmith et al. (2020) reports that SARS CoV-2 viruses are spherical in shape, and the structure is surrounded by dark dots, which might have been interpreted as spikes on coronavirus. The transmission electron microscope image also showed the spherical shape of the SARS CoV-2 virus. SARS CoV-2 aerosols are injected beginning from the inlet surface in the normal direction. The mass flow rate at the inlet is 0.5003 kg/s.The particles are injected from the inlet surface area, and each face of the surface inject a single particle. The particle distribution at the inlet surface is uniform, and all particles are injected at once. A total 14800 particles were injected. The outlet boundary condition is used as pressure outlet, and open pressure condition is used at the terminal outlets.

The SARS CoV-2aerosols were considered as secondary phase, and the air was the continuous phase. The interaction between discrete phase and continuous phase is considered. The maximum number of steps of tracking parameters is 5x10^{-8} and the step length factor is 5. Crowe et al. (2011) calculated the particle momentum response and collision time ratio, which eventually indicated whether the air was dilute or dense.

The momentum response time of the particle can be explained as;

$$\tau_V = \frac{\rho_p d_p^{\,2}}{18\mu} \quad (10)$$

where particle density is ρ_p, particle diameter is d_p, and μ is the viscosity of air.

The time between the collisions can be defined as;

$$\tau_c = \frac{1}{n\pi d_p^{\,2} v_r} \quad (11)$$

where n is the particle number, v_r is the particle relative velocity. If the ratio value is less than one, the fluid is dilute and one-way coupling can be considered. The value obtained for the ratio in the present study was 0.00041, which meant that this study is a one-way.

This study used 'trap' boundary condition for the wall. The physical meaning of the 'trap' condition' is particle will stick on the wall once it touches the wall. Once the particle touches the airway wall, the trajectory calculations will be terminated, and the fate of the particle will be recorded as 'trapped'. The deposition fraction is defined as;

$$\text{DF} = \frac{\text{Number of deposited particles in the wall}}{\text{Number of virus particles entering the inlet}}$$

Grid Refinement and Model Validation

A 17-generation airway model (Gemci et al. 2008; Schmidt et al. 2004) is employed for the SARS CoV-2 aerosol transport and deposition to the lower part of the lung. Figure 1 shows the airway model with five different lobes. The study performed a proper grid refinement, the details of the mesh at different section of the airway as well as the details of the grid refinement can be found in author's previous study (Islam et al. 2018).

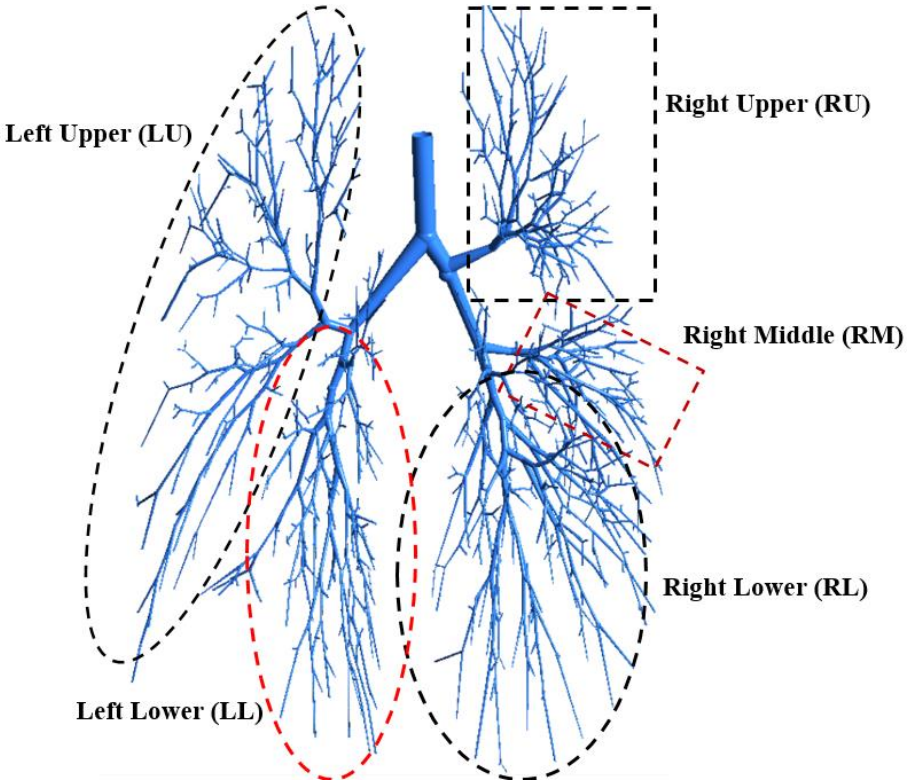

Figure 1: Highly asymmetric 5-lobes 17-generation human lung model

The numerical approach is validated with the available experimental and computations measurement in literature. A range of ultrafine particles are used to validate the deposition fraction (DF) at the upper airways. The ultrafine particle transport and DF is calculated for different airflow rates. Figure 2 illustrates the DF of the present calculation at 10 L/min inlet conditions with available literature data. The overall DF of the present study shows a close match with the available experimental and numerical measurements.

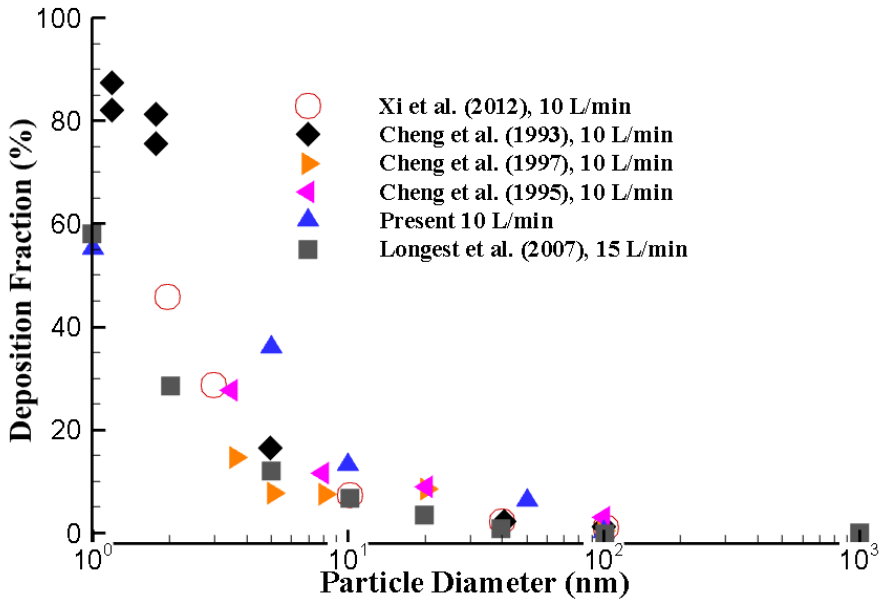

Figure 2: Numerical results validation with available literature at 10 L/min inlet airflow .

The DF of the present approach at higher flow rate is also comparing with the existing literature (Cheng et al. 1996; Cheng et al. 1995; Cheng et al. 1993; Longest, Xi and Technology 2007; Xi et al. 2012). Figure 3 demonstrates the comparison of DF at 20 L/min flow rate at the upper airways. The DF for the smaller diameter particle is found to be higher when comparing to the larger diameter nano-particle, which also support the hypothesis of the Brownian motion. The DF of this present calculation indicates an good agreement with the available results for larger nano-size particles .

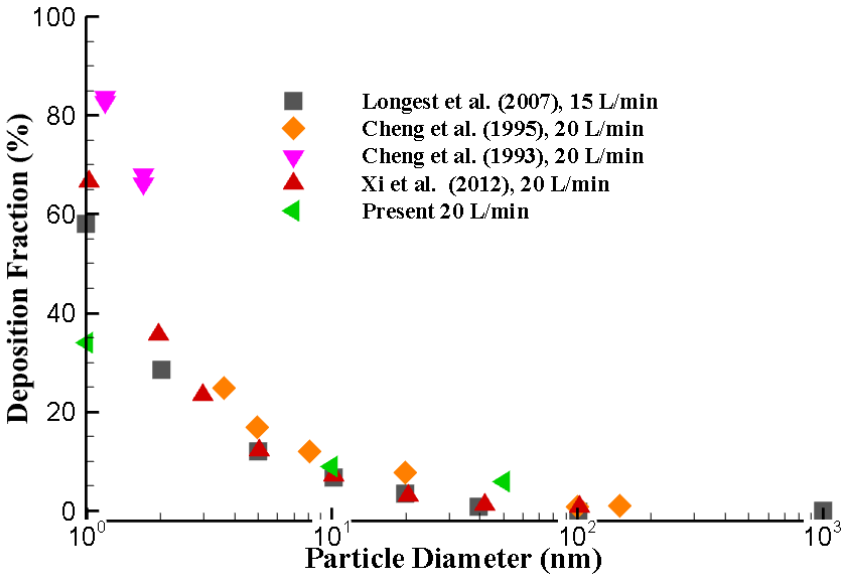

Figure 3: Numerical results validation with available literature at 20 L/min inlet flow (Cheng et al. 1995; Cheng et al. 1993; Longest, Xi and Technology 2007; Xi et al. 2012).

Results and Discussion

The airflow and SARS CoV-2 aerosol transport to the lower part of lung are simulated for different inlet conditions. A highly asymmetric 17-generation bifurcating model is utilised to analyse the SARS CoV-2 aerosol transport and deposition to the lower airways. The overall investigation is performed for three different airflow rates, which consist of 7.5 L/min, 15 L/min, and 30 L/min.

The velocity profiles are plotted at various positions of the upper airways, and the lung at the left side and right side for different breathing conditions. SARS CoV-2 aerosol usually follows the air streamline inside the respiratory tube. An accurate understanding of the upper and lower airways flow pattern is important to analyse the SARS CoV-2 transport and lung deposition. Figure 4 presents the velocity profiles for three different flow rates at selected cross-sections in different areas for the 17-generation lung model, from the trachea to terminal part of the lung. Figure 4a presents the velocity profiles at the trachea. Figure 4b-d presents the velocity

profiles at three lobes (upper, lower and middle) of the right lung. Figure 4e-f presents the velocity profiles at two lobes (lower and upper) of left lung.

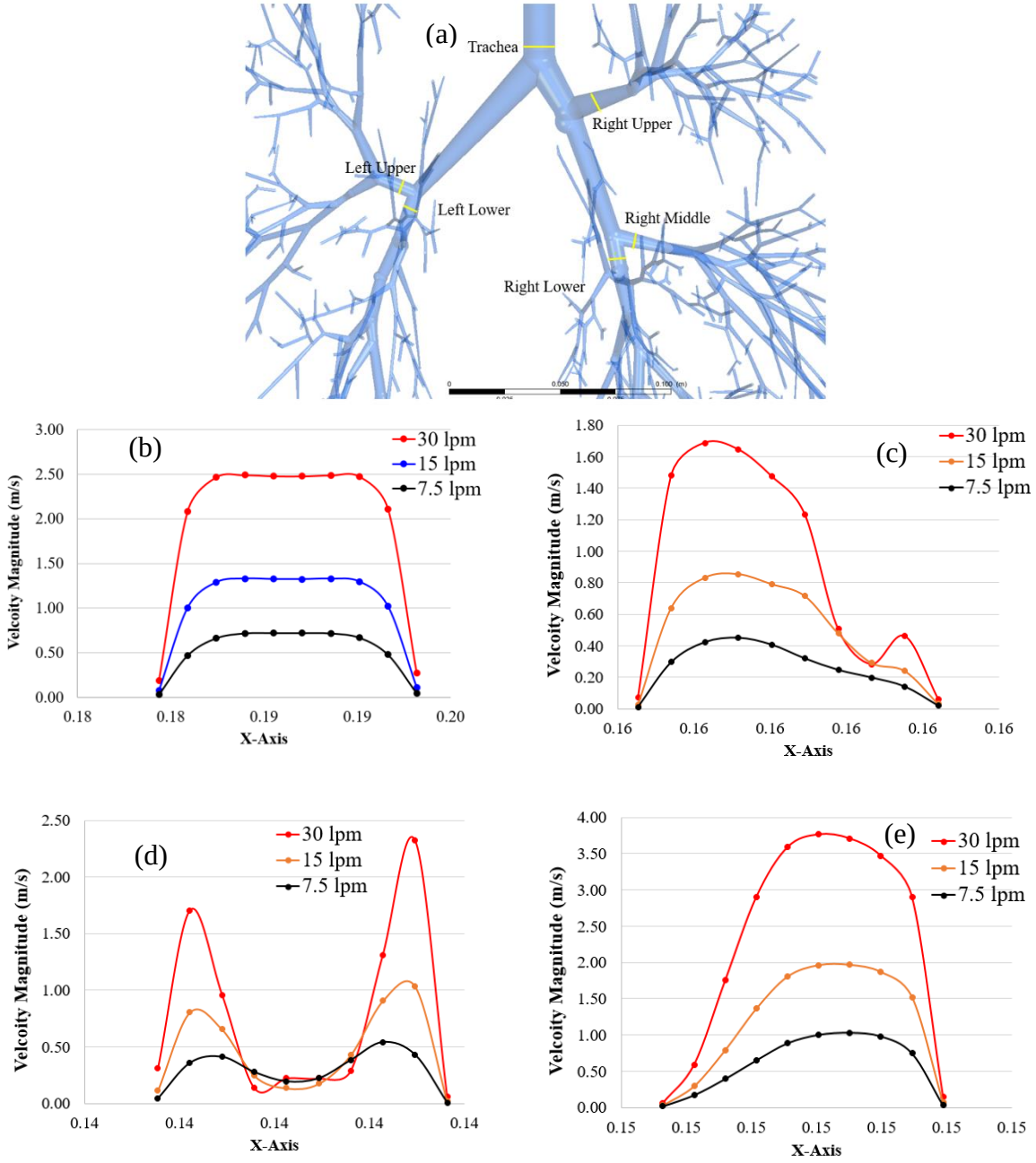

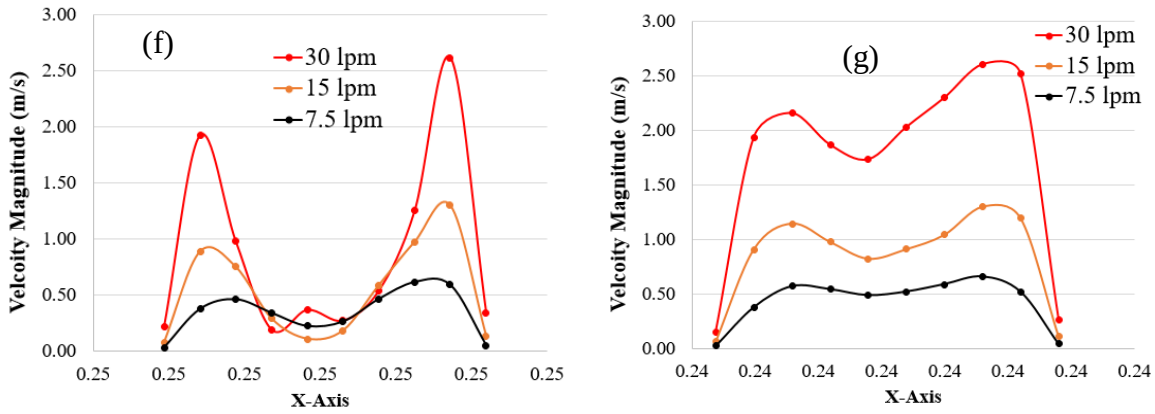

242

243 Figure 4: Air velocity profiles at randomly chosen location of the airway, (a) random location
244 definition, (b) trachea, (c) right upper (RU) lobe, (d) right middle (RM) lobe, (e) right lower
245 (RL) lobe, (f) left upper (LU) lobe and (g) left lower (LL) lobe.

246 Figure 4(a) shows the randomely selected locations at trachea and various lobes of the airway
247 model. The velocity profiles for all three airflow rates at the tracheal area show a fully
248 developed behaviour (Figure 4b) and the velocity magnitude is maximum at the centre of the
249 airways for all cases. However, the velocity field for all lobes tends to be locally transitional,
250 especially at RM lobe (Figure 4d) and LU lobe (Figure 4f), which have similar air velocity
251 magnitudes and nearly reach the 0.1 m/s at the middle point of the cross-section for all three
252 airflow rates. The velocity magnitude is higher close to the airway wall for RM and LU lobes,
253 which potentially increases the SARS CoV-2 aerosol deposition at the airways of the RM and
254 LU lobes. At the RU lobe, the velocity profile for 30 L/min shows a different trend than other
255 flow rates (Figure 4c). AT 30 L/min condition, the flow becomes locally unstable. The velocity
256 magnitude at the RL lobe (Figure 4e) is found maximum, whereas the RU lobe (Figure 4c) is
257 found to have the lowest velocity magnitude.

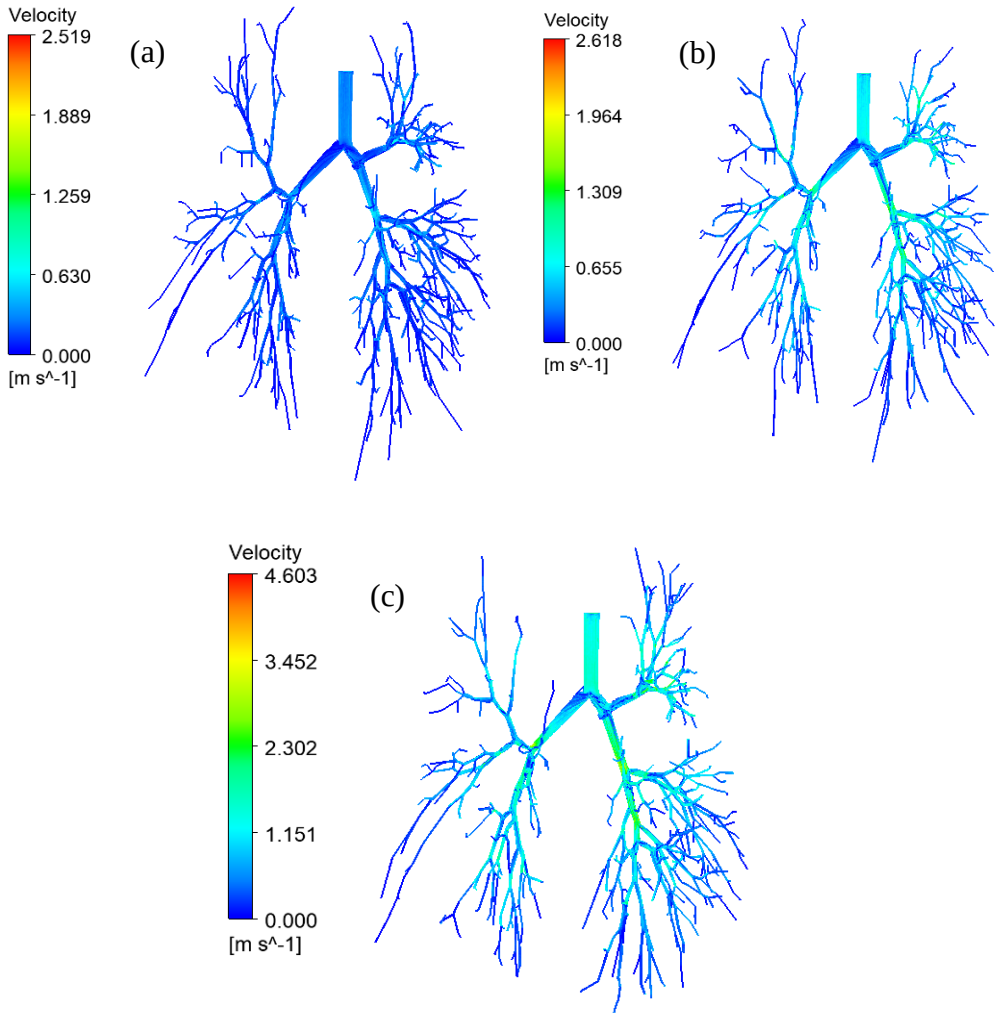

Figure 5: Velocity streamline at different airflow rates, (a) 7.5 L/min, (b) 15 L/min and (c) 30 L/min.

Figure 5 presents the velocity streamlines throughout the bifurcating model for various airflow rates. Figure 5a shows the air velocity streamlines at 7.5 L/min, whereas Figure 5b and 5c presents the air velocity streamline at 15 L/min and 30 L/min, respectively. The overall velocity streamline shows a higher velocity magnitude at the upper area of the bifurcating model. The velocity streamlines figure for low inlet velocity conditions (Figure 5a) indicates relatively low-velocity magnitude to the terminal bronchioles than the high-velocity conditions (figure 5c). For low inlet flow condition (Figure 5a), the highest velocity magnitude is reported at the upper bronchioles for all three right lobes. On the contrary, 15 L/min (Figure 5b) and 30 L/min (Figure 5c) have the highest air velocity at the initial area for all five main lobes.

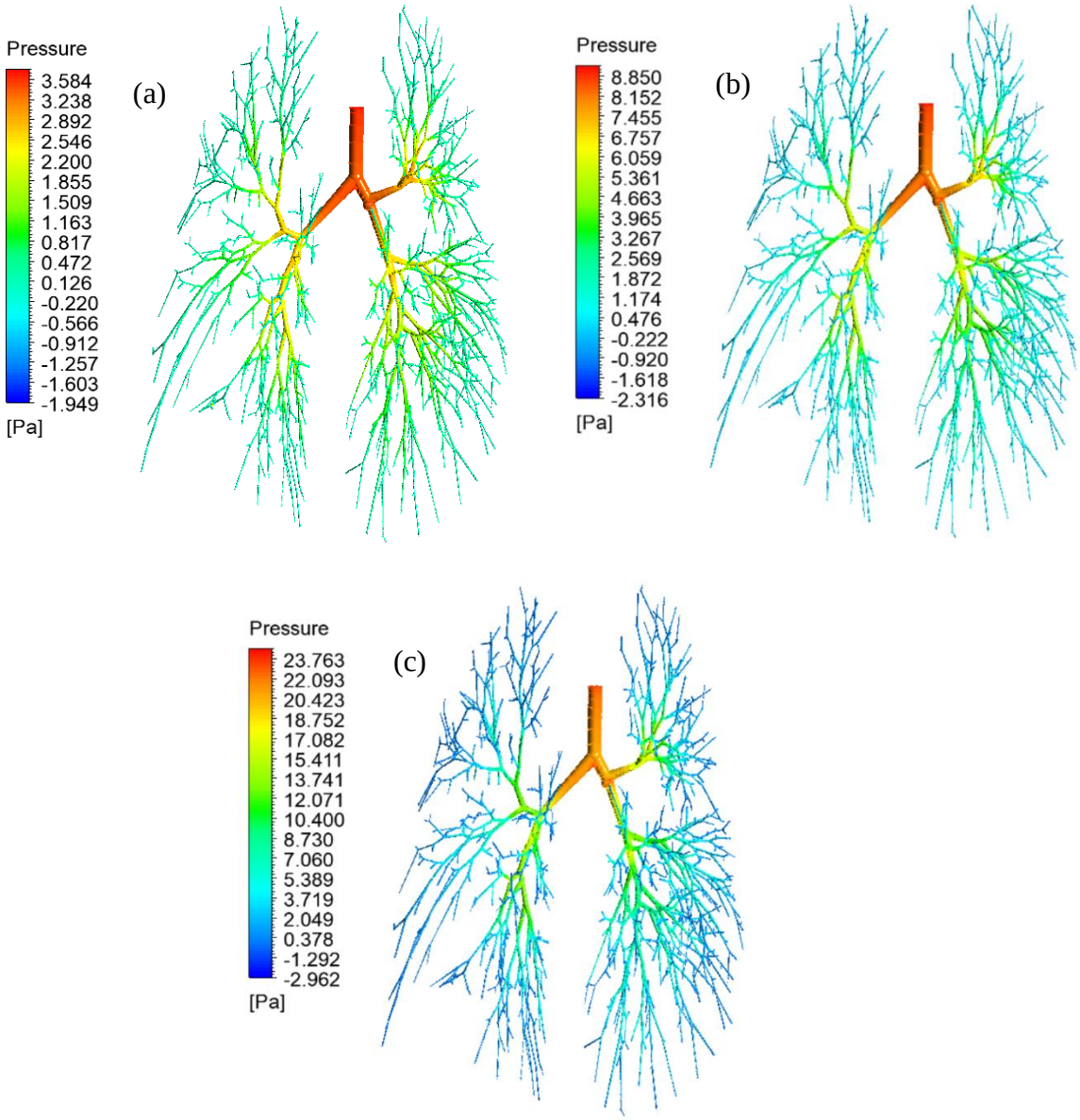

269 Figure 6: Pressure contour throughout the lung airways, (a) 7.5 L/min, (b) 15 L/min and (c)

270 30 L/min

271 The precise knowledge of the airway pressure and pressure-drop to the terminal airways is

272 important for airway health risk analysis. Figure 6 presents the pressure contours for all three

273 different airflow rates that include 7.5 L/min (Figure 6a), 15 L/min (Figure 6b), and 30 L/min

274 (Figure 6c). Figure 6 reports that the pressure generally decreases from the initial area (trachea)

275 to the lower generation (17^{th} generation). The pressure at the tracheal wall and the upper

276 airways is found maximum for all cases, and a significant pressure drop is obviously found in

277 the lower airways. The maximum pressure of 23.763 Pa is found at the highest airflow rate at

30 L/min (Figure 6c), while the maximum pressure of 3.584 Pa is found at the lowest airflow rate at 7.5 L/min (Figure 6a). Figure 6a shows, at low inlet condition (7.5 L/min), the pressure drop from the upper airways to the lower airways is insignificant. At high inlet velocity condition (30 L/min), the pressure drop is found significant from the upper airways to the lower airways. At high flow conditions, the terminal airways velocity magnitude is found relatively higher than the low inlet condition, which is reported in figure 5c. The higher velocity magnitude at the terminal airways eventually generates low pressure at the lower airways.

The SARS CoV-2 Aerosol deposition scenario is presented in Figure 7 under various airflow rate conditions. Figure 7a illustrates the deposition for airflow rate at 7.5 L/min, while Figure 7b, c shows the deposition for the airflow rate at 15 L/min and 30 L/min, respectively.

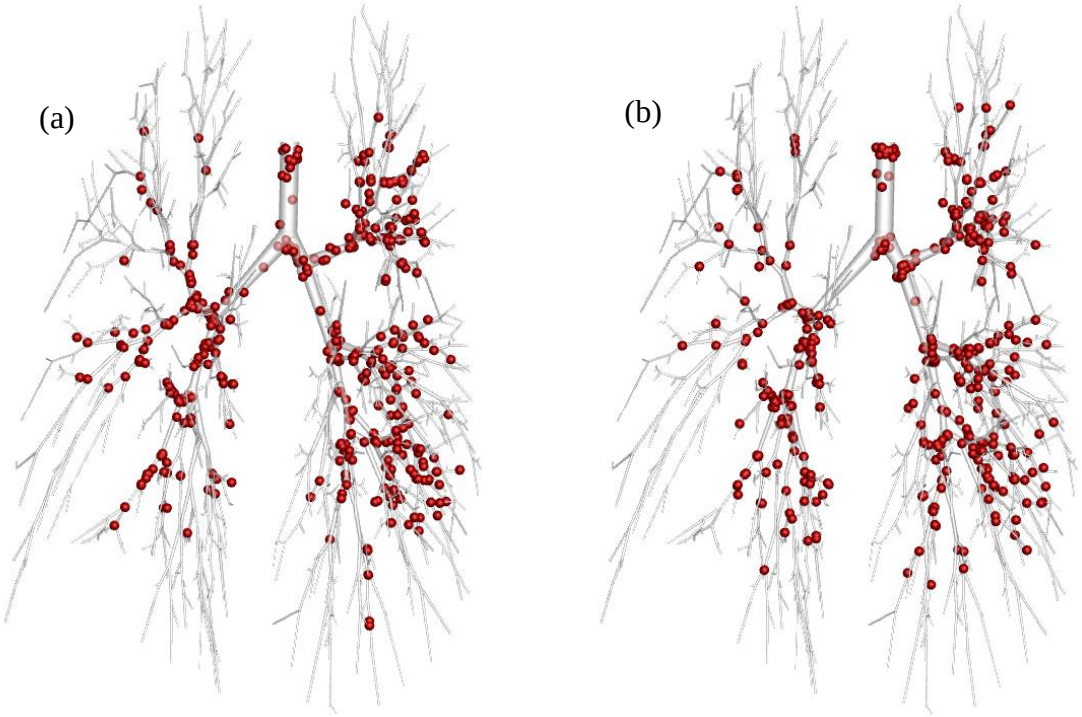

(c)

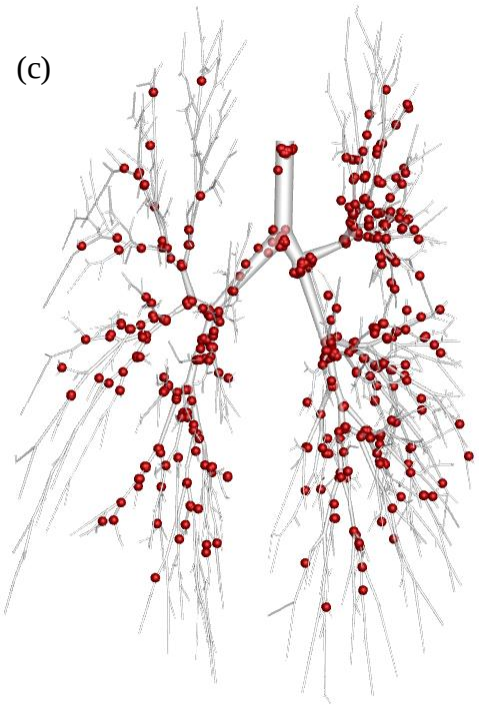

Figure 7: SARS CoV-2 Aerosol deposition (120nm) at different physical conditions, (a) 7.5 L/min, (b) 15 L/min and (c) 30 L/min flow rate. (Sphere size is increased during post-processing for visualisation purpose)

Figure 7 shows that the SARS CoV-2 Aerosols are more trapped in the tracheal area and the bifurcation of all generations in the lung lobes for both lung sides. Figure 7 shows the higher SARS CoV-2 aerosol which is trapped at the tracheal inlet, and upper airways at 7.5 L/min (Figure 7a) and 15 L/min (Figure 7b) compared to the airflow rate at 30 L/min (Figure 7c). Brownian motion effect is dominant for smaller aerosol like SARS CoV-2 transport and deposition. SARS CoV-2 aerosol can spontaneously transport through the airways at a low flow rate, and the random movement of the SARS CoV-2 aerosol increases the overall deposition rate at the upper airways. Simultaneously, the Brownian motion effect becomes less effective with the increase of the velocity magnitude. The SARS CoV-2 aerosol deposition at the right side is higher than the left side for all airflow rates. At 15 L/min (Figure 7b) and 7.5 L/min (Figure 7a) shows a cluster of SARS CoV-2 aerosol deposition at the three right lobes,

whereas the high airflow rate at 30 L/min (Figure 7c) shows a cluster SARS CoV-2 aerosol deposition at the upper area of the right side only.

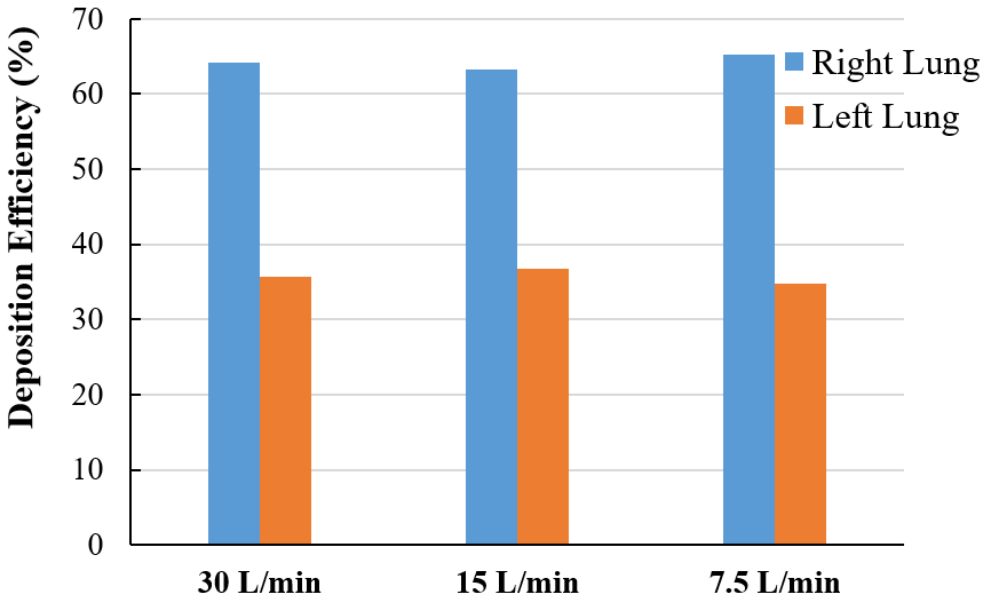

Figure 8: DE comparison at right and left lung for different airflow rate conditions.

Comparing SARS CoV-2 aerosol deposition efficiency (DE) between the right and the left lung is calculated and figure 8 reports the DE under the various airflow rate conditions. Figure 8 shows that the DE of the SARS CoV-2 aerosol at the left side is found to be lower when comparing to the right side for all airflow rates. At 7.5 L/min, the highest DE 65.22% is reported at the right lung, and the highest DE at the right lung causes the lowest DE at the left lung. At 30 L/min inlet case, the DE of the SARS CoV-2 aerosol in the lung at the right side is 64.25% and the left side is 35.75%. The anatomical structure of the right lung and left lung are different, and right lung airway diameter is higher than the left lung. A number of studies analysed the total flow distribution (%) in the right lung and left lung and found higher flow distribution to the right lung than the left lung. Cohen, Sussman and Lippmann (1990) found 60% of the total flow goes through the right lung, Horsfield et al. (1971) reports 54.6% of the total flow goes through the right lung, and Islam et al. (2018) reports 54.93% total flow goes

through the right lung. Higher flow distribution to the right lung indicates a higher amount of particle will go through the right bronchioles, which increases the deposition efficiency at the right lung. The SARS CoV-2 aerosol follows the air pathlines and more SARS CoV-2 aerosol enters into the right bifurcations due to high flow distribution to the right lung. The higher SARS CoV-2 aerosol in the right bifurcations increase the overall DE at the right lung.

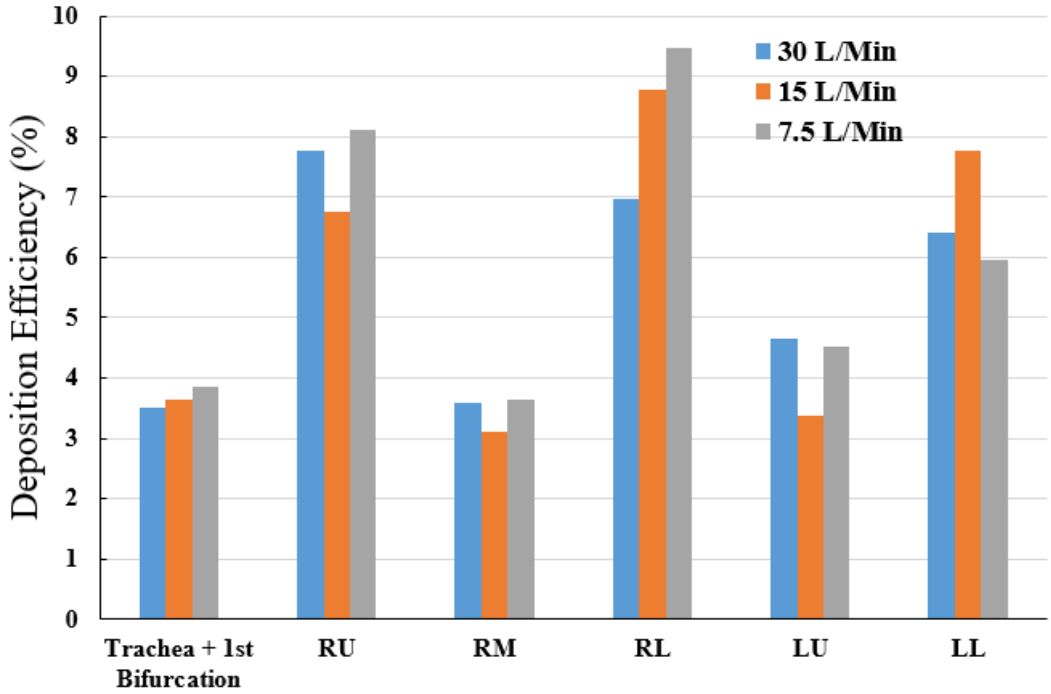

Figure 9: Local deposition of SARS CoV-2 Aerosol at different inlet conditions. LU, Left upper lobe; LL, left lower lobe; RU, right upper lobe; RM, right middle lobe; and RL, right lower lobe.

Figure 9 presents the SARS CoV-2 aerosol deposition at local areas involving the trachea & 1st bifurcation, the three lung lobes of the right side, and the two lung lobes of the left side. The local DE of the SARS CoV-2 aerosol is calculated for different airflow rates. The local DE of the SARS CoV-2 aerosol illustrates higher depsoition at the trachea and first bifurcation region at low inlet condition (7.5 L/min). At 7.5 L/min condition, 3.85% of the total SARS CoV-2 aerosols are deposited at trachea and first bifurcation area, whereas 3.51% SARS CoV-2

aerosols are deposited for 30 L/min case. The local SARS CoV-2 aerosol DE at the bronchioles of the RL lobe is found higher than other lobes. At 7.5 L/min inlet condition, 9.46% of the total SARS CoV-2 aerosols are deposited at the RL lobe, whereas 6.96% for 30 L/min airflow rate. At 15 L/min inlet case, the SARS CoV-2 aerosol deposition DE is found maximum at the LL lower lobe which is 7.77%. The overall SARS CoV-2 aerosol DE curve reports that the DE for 30 L/min inlet case is lower at all lobes, including the trachea and first bifurcation of the 17 generation model. For the comparison between the two lung sides, the overall DE at the right side is found to be higher than the left side. The DE at RM lobe and LU lobe is lower than other areas. To be concluded, the SARS CoV-2 aerosols are mostly trapped at RL lobe and RU lobe and rarely trapped at RM lobe and LU lobe for 7.5 L/min and 30 L/min. In contrast, for 15 L/min, the majority of the SARS CoV-2 aerosol deposition generally locates at RL lobe and LL lobe, while the minority of this aerosol deposition is in the RM lobe and LU lobe. The first-ever lob-specific SARS CoV-2, aerosol DE analysis for the 17-generation model, would improve the knowledge of the SARS CoV-2 transport to the lower part of the lung airways of a large-scale model. A Recent study have investigated the (Kwee and Kwee 2020b) CT-images of SARS CoV-2 positive patient from a RT-PCR test. The CT-Scan imaged reports the SARS CoV-2 presence at the RU lobe (figure 10a), RM and LL lobe (figure 10b), RU lobe (figure 10c) and both lower lobes (figire 10d), which necessarily indicate the significance of the present study. A comprehensive lob-specific analysis is presented in figure 9, which would potentially improve the knowledge of the field.

Figure 10 demonstrates the SARS CoV-2 aerosol deposition concentration in the right lung and left lung in the different airflow rate conditions. This aerosol deposition concentration is plotted based on the SARS CoV-2 aerosols x, y, z in the airway wall. Figure 10a presents the SARS CoV-2 aerosol concentration for 7.5 L/min flow condition at the right lung, while figure 10b shows the left lung concentration. Both figure's right panel shows the deposited SARS CoV-2

aerosol and the left panel shows the deposition concentration curve. The concentration curve on the left panel demonstrates the deposition hot spot at the bifurcating airways, that is presented at the right panel of the figure. The concentration curve shows the SARS CoV-2 aerosol deposition concentration is found to be higher at the upper as well as middle bifurcations of the 17-generation model. A comprehensive SARS CoV-2 aerosol deposition concentration for all cases are presented in figures 10 (c, d). At right lung, the SARS CoV-2 aerosol concentration shows a similar trent for all cases whereas a different trend is observed at the left lung. The asymmetric brunching pattern of the left and the right lung influences the overall SARS CoV-2 aerosol transport to the lower airways. This analysis would provide an understanding of the SARS CoV-2 aerosol deposition hot spot at the lower airways of a large model.

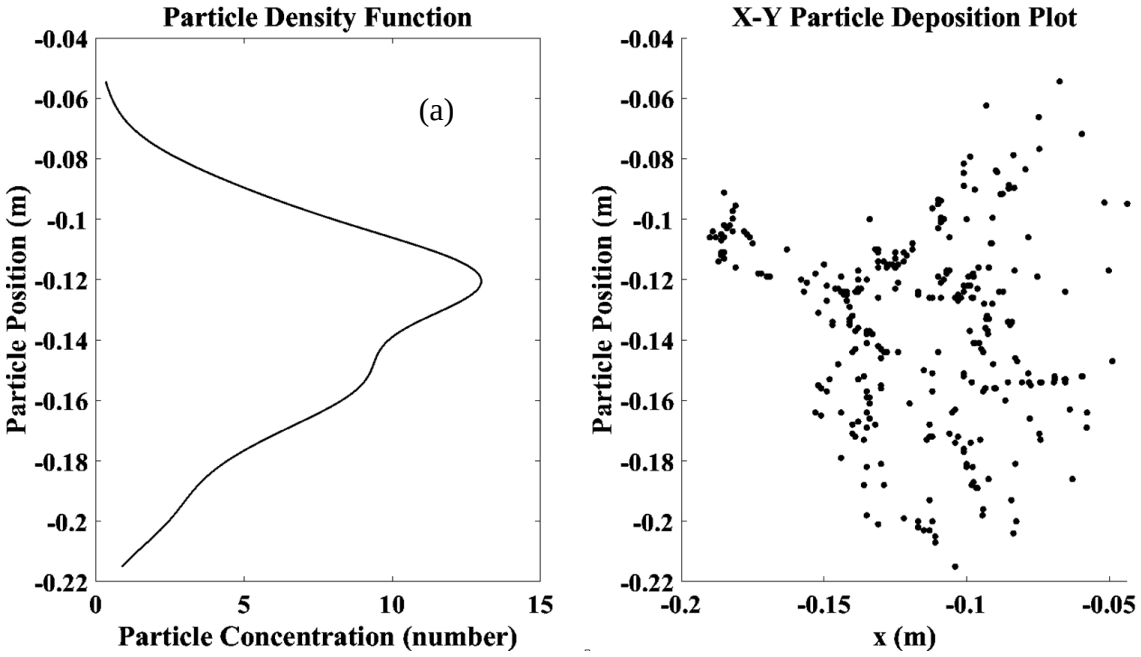

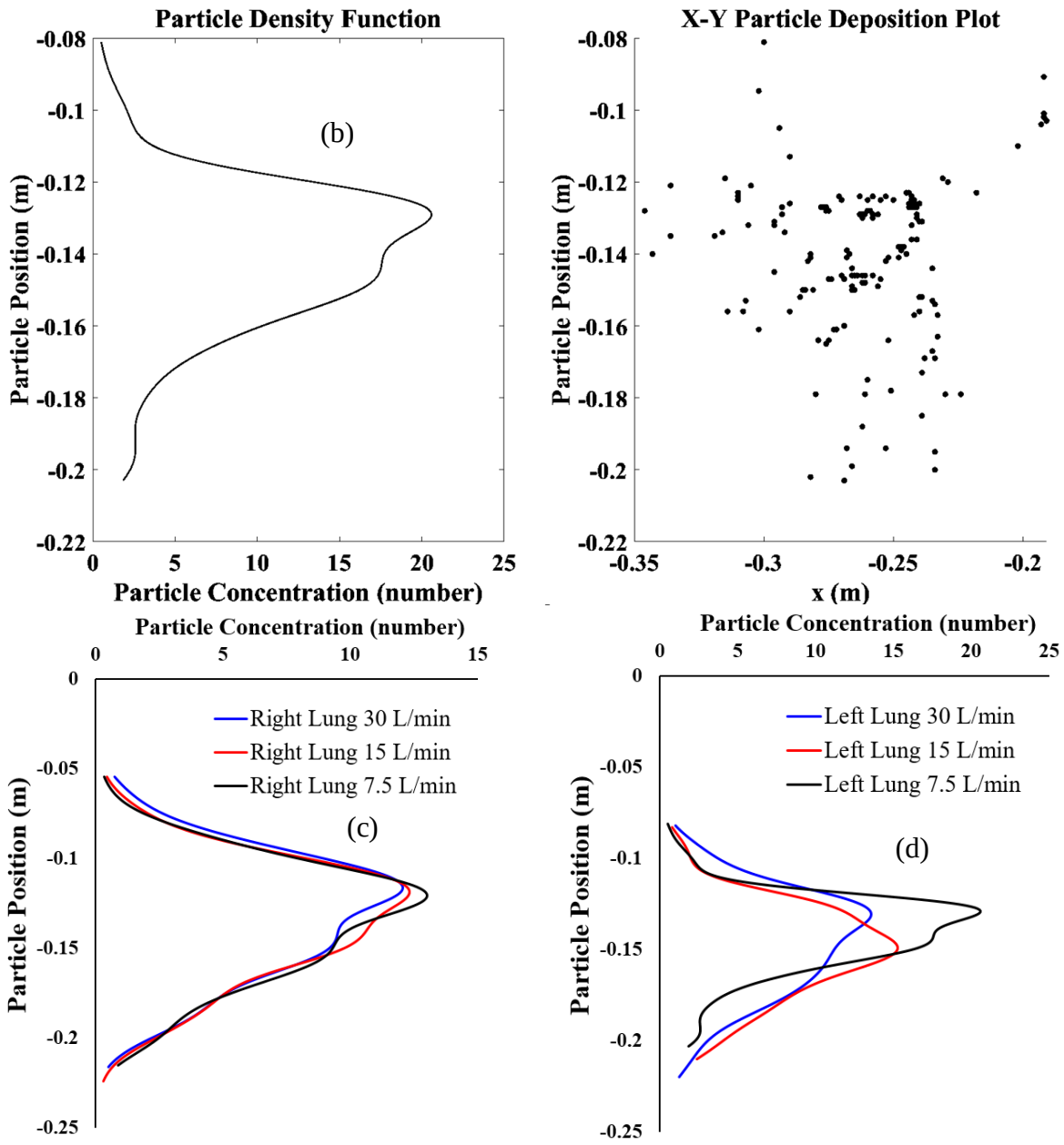

369

370 Figure 10: SARS CoV-2 aerosol deposition concentration from trachea to the terminal
371 airways for various airflow rate conditions, (a) 7.5 L/min at right lung, (b) 7.5 L/min at left
372 lung, (c) right lung, and (d) left lung.

373

374

375

Conclusions

In this paper, the SARS CoV-2 aerosol transport to the lower part of the lung airways of a 17-generations lung airway model is investigated numerically for the first time. The SARS CoV-2 aerosol transportation to the lower airways is investigated for different inlet conditions. The key findings of the study are listed as following;

- The cluster of SARS CoV-2 aerosols is found at the right lung, which is more than one time of the left lung for all airflow rates. A total of 35.55%, 33.45% and 32.90% of SARS CoV-2 injected aerosols are deposited to the airway wall for 7.5 L/min, 15 L/min and 30 L/min, respectively. The remaining aerosols escape and transport to lower generations and alveolar region.

- The highest deposition efficiency is located at the RL lobe with the low airflow rate of 7.5 L/min, whereas the lowest DE is found at the RM and LU lobes with the airflow rate of 15 L/min.

- The majority of SARS CoV-2 aerosols is trapped at RL and RU lobes, and the minority is trapped at RM and LU lobes for 7.5 L/min and 30 L/min airflow rates. For 15 L/min, the minority of aerosol deposition is in the RM and LU lobes which are similar to other airflow rates but the majority of this aerosol deposition is located at RL and LL lobes instead.

- The SARS CoV-2 deposition concentration curves show a similar trend for the right lung, while the left lung is different. The deposition hot spot (DHS) of the right lung is found at the first bifurcation of the RU lobe. For the left lung, the DHS is found at LU and LL lobes for 7.5 L/min and 30 L/min, while the 15 L/min has the DHS point at LU lobe only.

The numerical study demonstrates the SARS CoV-2 aerosol transport, and deposition concentration at different lobes of the large airway model. The numerical study investigated

the SARS CoV-2 aerosol transport to the lower area of the lung airways of a 17-generation model for the first time and a comprehensive lobe-specific analysis is performed, which would improve the SARS CoV-2 aerosol transport knowledge to the lower airways and help the health risk assessment of the covid patients. The numerical study also analysed the deposition hotspot of the SARS CoV-2 aerosol to the right and the left lung. The present study along with more patient-specific study would improve the knowledge of the field. The future study will investigate the age and patient-specific whole lung model for better understanding of the SARS CoV-2 aerosol to the lower airways.

Assumptions of the Study

In reality, the aerosol emitted during exhalation exhibits a wide size distribution. The smaller droplet could evaporate during transportation and become more smaller. During exhalation, the aerosol could contain a single SARS CoV-2 virus or more than one SARS CoV-2 virus. If the aerosol contains more than one SARS CoV-2 viruses, then the size and shape of the virus-laden particle could be different. This study assumed a single isolated virus and did not consider the aggregation of the SARS CoV-2 viruses. The future study will perform a comprehensive analysis on virus-laden particles, and the aggregation of the viruses on aged people lung as the virus is found deadly for older people. The study assumed that virus particles have no electrical charges for the intermolecular forces and van der Waals interactions are neglected as the study did not investigate the particle and lung surfactant interaction.

Conflicts of the Interest

No conflicts of interested are associated with this study.

Acknowledgement:

The authors thank the iHPC support at UTS. The 5th author thanks support from the Australian Research Council grants DP180103009 and IC190100020.

Data Availability:

The data that support the findings of this study are available from the corresponding author upon reasonable request.

References:

Anderson, P.J., 2005, History of Aerosol Therapy: Liquid Nebulization to MDIs to DPIs, Respiratory Care, vol. 50, no. 9, pp. 1139-1150.

Wells, W.F., 1955, Airborne contagion and air hygiene. Cambridge, MA: Harvard University Press.

Mason, R.J., 2020. Pathogenesis of COVID-19 from a cell biology perspective. Eur Respir Journal. vol. 55, pp. 1-3. doi: 10.1183/13993003.00607-2020

Atkinson, J.; Chartier, Y.; Pessoa-Silva, C. L.; Jensen, P.; Li, Y., Seto, W. (2009). Annex C: Respiratory droplets. *Natural Ventilation for Infection Control in Health-Care Settings*. World Health Organization. ISBN: 978-92-4-154785-7

Weibel, E.R., 1963, Morphometry of the Human Lung. Heidelberg: Springer Verlag.

Phillips, C.G., Kaye, S.R., 1995, Diameter-based analysis of the branching geometry of four mammalian bronchial trees. *Respiration Physiology*. vol. 102, pp. 303–316.

Kitaoka, H., Takaki, R., Suki, B. 1999, A three-dimensional model of the human airway tree. *Journal of Applied Physiology*. vol. 87, pp. 2207–2217.

Martonen, T.B., Yang, Y., Hwang, D., Fleming, J.S. 1995. Computer simulations of human lung structures for medical applications. *Computer Biology and Medicine*. vol. 25, pp. 431–446.

Lizal, F., Elcner, J., Hopke, P.K., Jedelsky, J., Jicha, M., 2012. Development of a realistic human airway model. Proc Inst Mech Eng H. vol. 226, no. 3, pp. 197-207. doi: 10.1177/0954411911430188.

Srivastav, V.K., Paul, A.R., Jain, A., 2013. Effects of cartilaginous rings on airflow and particle transport through simplified and realistic models of human upper respiratory tracts, Acta Mechanica Sinica, vol. 29, no. 6, pp. 883–892. doi: 10.1007/s10409-013-0086-2

Burrowes, K.S., Swan, A.J.,, Warren, N.J., Tawhai, M.H., 2008. Towards a virtual lung: multiscale, multiphysics modelling of the pulmonary system. *Philos Trans A Math Phys Eng Sci*. vol. 28, no. 366(1879), pp. 3247-63. doi: 10.1098/rsta.2008.0073.

Islam, M.S., Paul, G., Ong, H.X., Young, P.M., Gu, Y.T., Saha, S.C., 2020. A review of respiratory anatomical development, air flow characterisation and particle deposition, International Journal of Environmental Research and Public Health. vol. 17, no. 380, pp. 1-28.

Xi, J., Longest, P.W. 2007, Transport and deposition of micro-aerosols in realistic and simplified models of the oral airway. *Ann Biomed Eng.* vol. 35, no. 4, pp. 560-581. doi: 10.1007/s10439-006-9245-y

Islam, M.S., Saha,S.C., Sauret, E., Gemci, T., Gu, Y.T., 2017. Pulmonary aerosol transport and deposition analysis in upper 17 generations of the human respiratory tract, Journal of Aerosol Science, vol. 108, pp. 29-43.

Lizal, F., Elcner, J., Jedelsky, J., Maly, M., Jicha, M., Farkas, Á., Belka, M., Rehak, Z., Adam, J., Brinek, A., Laznovsky, J., Zikmund, T., Kaiser, J., 2020. The effect of oral and nasal breathing on the deposition of inhaled particles in upper and tracheobronchial airways. *J Aerosol Sci.* vol. 150:105649. doi: 10.1016/j.jaerosci.2020.10564

Kleinstreuer, C., Zhang, Z., Donohue, J.F., 2008. Targeted drug-aerosol delivery in the human respiratory system. *Annual Revision Biomedical Engineering*, vol. 10, pp. 195–220.

Martonen, T., Fleming, J., Schroeter, J., Conway, J., Hwang, D. 2003. In silico modeling of asthma. *Advanced Drug Delivery Reviews*. vol. 55, pp. 829-49, 2003.

Srivastav, V.K., Kumar, A., Shukla, S.K., Paul, A.R., Bhatt, A.D., Jain, A., 2014. Airflow and aerosol-drug delivery in a CT scan based human respiratory tract with tumor using CFD, *Journal of Applied Fluid Mechanics*. vol. 7, no. 2, pp. 345-356.

Kumar, S., Lee, H.P., 2020. The perspective of fluid flow behavior of respiratory droplets and aerosols through the facemasks in context of SARS-CoV-2. *Phys. Fluids*. vol. 32, 111301 (2020); doi: 10.1063/5.0029767

Prather, K. A., Wang, C. C., Schooley, R. T. 2020. Reducing transmission of SARSCoV-2, Science 368, 1422.

Vuorinen, V., Aarnio, M., Alava, M., Alopaeus, V., Atanasova, N., Auvinen, M., Balasubramanian, N., Bordbar, H., Erästö, P., Grande, R., Hayward, N., Hellsten, A., Hostikka, S., Hokkanen, J., Kaario, O., Karvinen, A., Kivistö, I., Korhonen, M., Kosonen, R., Kuusela, J., Lestinen, S., Laurila, E., Nieminen, H.J., Peltonen, P., Pokki, J., Puisto, A., Råback, P., Salmenjoki, H., Sironen, T., Österberg, M., 2020. Modelling aerosol transport and virus exposure with numerical simulations in relation to SARS-CoV-2 transmission by inhalation indoors. *Saf. Sci.* vol. 130, 104866.

Xie, X., Li, Y., Sun, H., Liu, L., 2009, Exhaled droplets due to talking and coughing. J. R. Soc., Interface. vol. 6, S703.

Feng, Y., Marchal, T., Sperry, T., Yi, H., 2020. Influence of wind and relative humidity on the social distancing effectiveness to prevent COVID-19 airborne transmission: A numerical study," J. Aerosol Sci. vol. 147, 105585.

Chaudhuri, S., Basu, S., Kabi, P., Unni, V.R., Saha, A., 2020. Modeling the role of respiratory droplets in COVID-19 type pandemics," Phys. Fluids. vol. 32, 063309.

Bhardwaj, R., Agrawal, A., 2020a. Likelihood of survival of coronavirus in a respiratory droplet deposited on a solid surface.Phys. Fluids. vol. 32, 061704 (2020) https://doi.org/10.1063/5.0012009

Bhardwaj, R., Agrawal, A., 2020b. How coronavirus survives for days on surfaces. Phys. Fluids, vol. 32, 111706. doi: 10.1063/5.0033306

Balázs G. Madas, Péter Füri, Árpád Farkas, Attila Nagy, Aladár Czitrovszky, Imre Balásházy, Gusztáv G. Schay, Alpár Horváth,2020. Deposition distribution of the new coronavirus (SARS-CoV-2) in the human airways upon exposure to cough-generated aerosol.medRxiv 2020.05.13.2010005 doi: 10.1101/2020.05.13.20100057

Koblinger, L., Hofmann, W., 1990. Monte Carlo modeling of aerosol deposition in human lungs. Part I: Simulation of particle transport in a stochastic lung structure. Journal of Aerosol Science. vol. 21, pp. 661–674. doi:10.1016/0021-8502(90)90121-D

Fitzpatrick, M.F., McLean, H., Urton, A.M., Tan, O'Donnell, D., Driver, H.S., 2003. Effect of nasal or oral breathing route on upper airway resistance during sleep. European Respiratory Journal. vol. 22, pp. 827-832; DOI: 10.1183/09031936.03.00047903

Fernández Tena A, Casan Clarà P., 2012. Deposition of Inhaled Particles in the Lungs.Arch Bronconeumol. 2012;48(7):240–246

Mortazavi, H., Mortazavy Beni, H., Aghaei, F., Sajadian, S.H., 2020. SARS-CoV-2 droplet deposition path and its effects on the human upper airway in the oral inhalation. Computer Methods and Programs in Biomedicine. https://doi.org/10.1016/j.cmpb.2020.105843

Heyder, J.. 2004. Deposition of Inhaled Particles in the Human Respiratory Tract and Consequences for Regional Targeting in Respiratory Drug Delivery. Proc Am Thorac Soc. vol. 1. pp 315–320. DOI: 10.1513/pats.200409-046TA

Frederix, E.M.A., Kuczaj, A.K., Nordlund, M., Bělka, M., Lizal, F., Jedelský, J., Elcner, J., Jícha, M., Geurts, B.J., Simulation of size-dependent aerosol deposition in a realistic model of the upper human airways. Journal of Aerosol Science 115 (2018) 29–45https://doi.org/10.1016/j.jaerosci.2017.10.007

Pozin, N. 2017. Multiscale lung ventilation modeling in health and disease. Modeling and Simulation. Université Pierre et Marie Curie - Paris VI, 2017. English. ffNNT: 2017PA066581ff.

https://www.nih.gov/news-events/nih-research-matters/novel-coronavirus-structure-reveals-targets-vaccines-treatments (access on 5th May 2021)

Ciloglu, D., A numerical study of the aerosol behavior in intra-acinar region of a human lung. 2020. Phys. Fluids 32, 103305 (2020); https://doi.org/10.1063/5.0024200

Munir, B., Xu, Y., 2020. Effects of gravity and surface tension on steady microbubble propagation in asymmetric bifurcating airways. Phys. Fluids 32, 072105 (2020); https://doi.org/10.1063/5.0012796

Xi, J., Si, X.A., Nagarajan, R., 2020. Effects of mask-wearing on the inhalability and deposition of airborne SARS-CoV-2 aerosols in human upper airway. Phys. Fluids 32, 123312 (2020); https://doi.org/10.1063/5.0034580

Mallik, A.K., Mukherjee, S., Panchagnula, M.V., 2020. An experimental study of respiratory aerosol transport in phantom lung bronchioles. Phys. Fluids 32, 111903 (2020); https://doi.org/10.1063/5.0029899

Zhou, M., Zou, J., 2021. A dynamical overview of droplets in the transmission of respiratory infectious diseases. Phys. Fluids 33, 031301 (2021); https://doi.org/10.1063/5.0039487

Si, X.A., Talaat, M., Xi, J., 2021. SARS COV-2 virus-laden droplets coughed from deep lungs: Numerical quantification in a single-path whole respiratory tract geometry. Phys. Fluids 33, 023306 (2021); https://doi.org/10.1063/5.0040914

Chaudhuri, S., S. Basu, P. Kabi, V. R. Unni, A. J. P. o. F. Saha. 2020. Modeling the role of respiratory droplets in covid-19 type pandemics 32:063309. doi.

Cheng, K.-H., Y.-S. Cheng, H.-C. Yeh, R. A. Guilmette, S. Q. Simpson, Y.-H. Yang, D. L. J. A. S. Swift. 1996. In vivo measurements of nasal airway dimensions and ultrafine aerosol deposition in the human nasal and oral airways. *J Journal of Aerosol Science* 27:785-801. doi.

Cheng, K.-H., Y.-S. Cheng, H.-C. Yeh, D. L. J. A. S. Swift, Technology. 1995. Deposition of ultrafine aerosols in the head airways during natural breathing and during simulated breath holding using replicate human upper airway casts. *J Aerosol Science* 23:465-474. doi.

Cheng, Y.-S., Y.-F. Su, H.-C. Yeh, D. L. J. A. S. Swift, Technology. 1993. Deposition of thoron progeny in human head airways. *J Aerosol Science* 18:359-375. doi.

Cohen, B. S., R. G. Sussman, M. Lippmann. 1990. Ultrafine particle deposition in a human tracheobronchial cast. *Aerosol Science and Technology* 12:1082-1091. doi.

Crowe, C. T., J. D. Schwarzkopf, M. Sommerfeld, Y. Tsuji. 2011. *Multiphase flows with droplets and particles*: CRC press.

Gemci, T., V. Ponyavin, Y. Chen, H. Chen, R. Collins. 2008. Computational model of airflow in upper 17 generations of human respiratory tract. *Journal of Biomechanics* 41:2047-2054. doi.

Goldsmith, C. S., S. E. Miller, R. B. Martines, H. A. Bullock, S. R. Zaki. 2020. Electron microscopy of sars-cov-2: A challenging task. *J The Lancet* 395:e99. doi.

Haider, A. and O. J. P. t. Levenspiel. 1989. Drag coefficient and terminal velocity of spherical and nonspherical particles. *J Powder technology* 58:63-70. doi.

Horsfield, K., G. Dart, D. E. Olson, G. F. Filley, G. Cumming. 1971. Models of the human bronchial tree. *Journal of applied physiology* 31:207-217. doi.

https://www.pptaglobal.org/media-and-information/ppta-statements/1055-2019-novel-coronavirus-2019-ncov-and-plasma-protein-therapies. doi.

Inthavong, K., J. Tu, G. Ahmadi. 2009. Computational modelling of gas-particle flows with different particle morphology in the human nasal cavity. *The Journal of Computational Multiphase Flows* 1:57-82. doi.

Islam, M. S., S. C. Saha, T. Gemci, I. A. Yang, E. Sauret, Y. T. Gu. 2018. Polydisperse microparticle transport and deposition to the terminal bronchioles in a heterogeneous vasculature tree. *Scientific Reports* 8:16387. doi: 10.1038/s41598-018-34804-x.

Kwee, T. C. and R. M. Kwee. 2020a. Chest ct in covid-19: What the radiologist needs to know. *J RadioGraphics* 40:1848-1865. doi.

Kwee, T. C. and R. M. Kwee. 2020b. Chest ct in covid-19: What the radiologist needs to know. *J RadioGraphics* 40:1848-1865. doi.

Longest, P. W., J. Xi, Technology. 2007. Effectiveness of direct lagrangian tracking models for simulating nanoparticle deposition in the upper airways. *J Aerosol Science* 41:380-397. doi.

Schmidt, A., S. Zidowitz, A. Kriete, T. Denhard, S. Krass, H.-O. Peitgen. 2004. A digital reference model of the human bronchial tree. *Computerized Medical Imaging and Graphics* 28:203-211. doi: http://dx.doi.org/10.1016/j.compmedimag.2004.01.001.

White, F. M. 2003. Fluid mechanics. 5th. *Boston: McGraw-Hill Book Company*. doi.

589 Xi, J., A. Berlinski, Y. Zhou, B. Greenberg, X. J. A. o. b. e. Ou. 2012. Breathing resistance and ultrafine
590 particle deposition in nasal–laryngeal airways of a newborn, an infant, a child, and an adult. *J*
591 *Annals of biomedical engineering* 40:2579-2595. doi.

592
593